Journal of
Composites Science

MDPI

Article

The Mechanism of Joint Reduction of MoO_3 and CuO by Combined Mg/C Reducer at High Heating Rates

Hasmik Kirakosyan [1,*], Khachik Nazaretyan [1], Sofiya Aydinyan [1,2] and Suren Kharatyan [1]

[1] A.B. Nalbandyan Institute of Chemical Physics NAS RA, P. Sevak 5/2, Yerevan 0014, Armenia; khachik.nazaretyan@ichph.sci.am (K.N.); sofiya.aydinyan@taltech.ee (S.A.); suren@ichph.sci.am (S.K.)
[2] Department of Mechanical and Industrial Engineering, Tallinn University of Technology, Ehitajate 5, 19086 Tallinn, Estonia
* Correspondence: hasmik.kirakosyan@ichph.sci.am; Tel.: +374-9418-1606

Abstract: Understanding of the decisive role of non-isothermal treatment on the interaction mechanism and kinetics of the MoO_3-CuO-Mg-C system is highly relevant for the elaboration of optimal conditions at obtaining Mo-Cu composite powder in the combustion processes. The reduction pathway of copper and molybdenum oxides with combined Mg + C reducing agents at high heating rates from 100 to 5200 K min^{-1} was delivered. In particular the sequence of the reactions in all the studied binary, ternary and quaternary systems contemporaneously demonstrating the effect of the heating rate on products' phase composition and microstructure was elucidated. The combination of two highly exothermic and speedy reactions (MoO_3 + 3Mg and CuO + Mg vs. MoO_3 + CuO + 4Mg) led to a slow interaction with weak self-heating (dysynergistic effect) due to a change in the reaction mechanism. Furthermore, it has been shown that upon the simultaneous utilization of the Mg and C reducing agents, the process initiates exclusively with carbothermic reduction, and at relatively high temperatures it continues with magnesiothermic reaction. The effective activation energy values of the magnesiothermic stages of the studied reactions were determined by Kissinger isoconversional method.

Keywords: non-isothermal kinetics; joint reduction of oxides; high heating rate; Mg/C combined reducer; dysynergistic effect; activation energy

Citation: Kirakosyan, H.; Nazaretyan, K.; Aydinyan, S.; Kharatyan, S. The Mechanism of Joint Reduction of MoO_3 and CuO by Combined Mg/C Reducer at High Heating Rates. *J. Compos. Sci.* **2021**, *5*, 318. https://doi.org/10.3390/jcs5120318

Academic Editor: Francesco Tornabene

Received: 3 November 2021
Accepted: 21 November 2021
Published: 3 December 2021

1. Introduction

W, Mo and their multicomponent alloys are nominated as potential candidates for plasma facing materials (PFMs) simultaneously possessing high melting temperature, high thermal conductivity, thermal fatigue, low vapor pressure and low sputtering erosion yield [1–3]. Copper is considered the heat-sink component for nuclear fusion devices due to its good thermal conductivity [3–5]. The conventional welding of refractory metal (such as W, Mo) and Cu is an extremely difficult task caused by their immiscibility in both solid and liquid states [6–9], which can be alleviated through the utilization of well-mixed and dispersed components. The simultaneous synthesis of components of Mo-Cu composite alloy may guarantee the connection of Mo/Cu and promote high-tech development of thermonuclear fusion energy applications. Self-propagating exothermic reaction (SHS) for synthesizing composite materials and intermetallic compounds has already shown its effectiveness [10–12] in an in situ preparation of Mo-Cu composite powder by coreduction of metal oxide precursors via reaction's coupling approach [13,14]. Detailed knowledge on the high speed and high-temperature kinetics of MoO_3-CuO-Mg-C system during the SHS reaction is of high importance not only for the elaboration of optimal conditions at obtaining Mo-Cu composite powder, but also extending the obtained models and interpretation on the similar systems. However, the intensive nature of exothermic SHS reactions, with the heating rate of over 10^2 K s^{-1} make it difficult to explore the interaction mechanism of condensed constituents (solid, liquid) in the combustion wave. The modeling of the

combustion process at controllable conditions (e.g., with programmed heating rates and tuning the process within the time at conditions closer to heating rates and temperatures in the combustion wave) will tackle the examination of the reaction pathway. The latter was studied so far by means of X-ray diffraction, electron microscopy and thermal analysis techniques without consideration the influence of high heating rates on the interaction dynamics. Motivated by the open questions and technical difficulties of combustion kinetics exploration, our current study is aimed to disclose the interaction pathway at high heating rates in the MoO_3-CuO-Mg-C system by a novel thermal analysis technique, called high-speed temperature scanner (HSTS) [15–18].

HSTS studies are suitable for the solid–solid and solid–liquid intercollisions that are unquestionably the most abundant among nature's phase transformations [19,20]. It has already proved its ability to find out transformations and transitions in alloys, ceramic and composite materials. Our recent findings via HSTS technique [21] provided valuable knowledge about intermediate states of solid and liquid phases, their nucleation processes, phase and structure formation pathways in condensed phase at heating rates from 100 to 2500 K s^{-1} region. In [22] the mechanism and kinetics of reactions in the MoO_3-CuO-Mg-C system has been investigated at non-isothermal conditions by DTA/TG method at low heating rates (5–20 K min^{-1}) up to 1273 K. The current work is the consequential extension of the investigation of the reaction mechanism in CuO-MoO_3-Mg-C powder mixtures from 100 up to 5200 K min^{-1} high heating conditions up to 1573 K. The technique of local non-isothermal high heating enables us to study the sequence of concurrent reduction processes of strictly different oxides, reveal the not obvious reduction mechanism with an Mg/C reductant pair, the effect of heating rate on the phase and structure formation patterns and conversion degree. The multistep transformations in the CuO-MoO_3-Mg-C powder mixtures were demonstrated to be significantly influenced by the formation of intermediate molybdates, even up to the drastic change in reaction pathway. Furthermore, the comparative overview of reactions' sequences in a wide range of heating rates and Arrhenius kinetic parameters allowed us to directly identify beneficial conditions, to study the main facets of the phases involved in each stage, and indicate a favorable direction in the design of the reduction process.

2. Materials and Methods

MoO_3 (High grade, Pobedit Company, Vladikavkaz, Russia, particle size < 15 μm), CuO (High grade, STANCHEM, Niemce, Poland, particle size < 40 μm), carbon black (P-803, Ivanovo carbon black and rubber JSC, Ivanovo, Russia, particle size < 1 μm) and magnesium (MPF-3, Ruskhim, Moscow, Russia, particle size 150–300 μm) powders were used as precursors for HSTS experiments (Figure S1).

The mechanism of reduction of copper and molybdenum oxides mixture by Mg/C combined reducers under conditions of high heating rates was investigated by HSTS technique. It allows to carry out experiments in a wide range of heating rates (from 10 to 10,000 K min^{-1}) up to 1573 K. The HSTS operation is based on the direct electric heating of thin metallic foil (e.g., Ni foil with 0.05–0.1 mm thickness). The small amount of powder (about 50 mg) was placed inside the middle part of thin metallic heater and then was heated by direct electrical current in the HSTS reaction chamber (Figure 1). Before heating, the chamber was sealed, evacuated and filled with argon up to 0.1 MPa pressure (Ar, 99.98% purity, oxygen < 0.01%). Preprogrammed heating mode was used to heat the sample. The temperature change (up to 1573 K) was recorded using a K type chromel-alumel thermocouple fixed in the central area of the foil and using a photocell fixed to the reactor wall. The inert experiment was characterized by linear temperature-time history defined by the given heating rate and coinciding with the reactive temperature profile where interactions are absent. The reaction onset temperature (T_o), the maximum peak temperature due to self-heating (T_{max}) and the temperature prescribed by linear heating (where the maximum exothermic effect is observed (T*)) were determined from the heating thermograms [21].

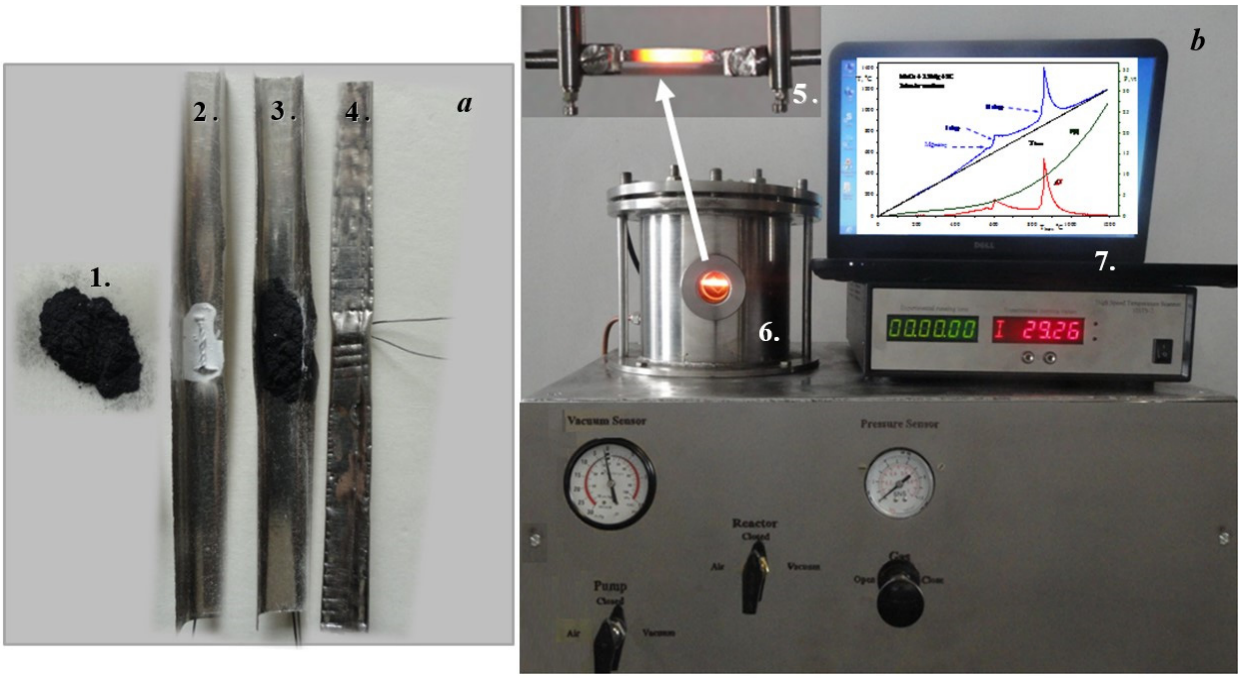

Figure 1. The experimental steps for the kinetic studies using high-speed temperature scanner. (**a**) Envelope heater with reactive mixture under study; (**b**) reaction chamber and controller: 1—reactive mixture, 2—boat made from nickel foil, 3—powder mixture in Ni boat, 4—envelope with mixture and thermocouple wire, 5—heated sample, 6—reaction chamber, 7—electronic unit and PC for control and registration.

During the heating, the process was interrupted at characteristic temperatures and the quenched samples were subjected to XRD analysis (diffractometer DRON-3.0, IC Burevestnik, St. Petersburg, Russia, CuKα radiation, 25 kV, 10 mA). Not that, the samples were cooled with high cooling rate (up to 12,000 K min^{-1}) to exclude further interactions. XRD patterns of the quenched samples can be viewed in Supplementary Figures. Besides, for the characterization of the samples cooled at characteristic temperatures, the IR spectral analysis (PerkinElmer Spectrum Two FT-IR, TL8000) was utilized. The effective activation energy values of magnesiothermic reduction stage in a heating rate region of 100–1200 K min^{-1}, were determined by the Kissinger isoconversional method for the studied binary (MoO_3-Mg), ternary (MoO_3-Mg-C) and quaternary (MoO_3-CuO-Mg-C) mixtures. For microstructural analysis, a field-emission scanning electron microscope (FE-SEM, Zeiss Evo MA15, Germany) equipped with an EDS (energy dispersive spectroscopy) detector was used.

3. Results and Discussion

The joint reduction of MoO_3 and CuO utilizing Mg + C combined reducer via energy-saving combustion synthesis aimed at the preparation of composite materials with fine and well-dispersed constituents was documented in [13,23,24], The advantage of such a reducing mixture is to govern the reaction thermal regime in a wide range of temperature and to prepare Mo-Cu composite powders in controllable combustion conditions. As it is difficult to disclose the interaction mechanism at extreme conditions of the combustion wave, the process was preliminarily modeled at "soft" conditions (e.g., low heating rates) using the DTA/TG technique [22] under programmed heating rates from 5 to 20 K min^{-1} up to 1273 K. Furthermore, to monitor and reveal mechanism of the combustion reaction due to its high velocity is still a challenge. Here we report the results of study of the reaction mechanism in CuO-MoO_3-Mg-C powder mixtures under conditions of high heating rates (from 100 to 5600 K min^{-1}) up to temperature 1573 K through revealing reactions' sequences and the phase- and microstructure formation patterns by HSTS-1 setup. Firstly, the reduction pathways were studied in binary (CuO-MoO_3, MoO_3-Mg,

MoO_3-C, CuO-C) and ternary (MoO_3-Mg-C, MoO_3-CuO-Mg, and MoO_3-CuO-C) systems, then the quaternary CuO-MoO_3-Mg-C system under the same heating conditions. The mechanism of copper oxide reduction under fast heating conditions both with Mg and (Mg + C) reducers is detailed in [21] and here that results are presented for the purpose of comparative discussion.

3.1. CuO-MoO_3, CuO-C, MoO_3-C, MoO_3-Mg Binary Systems

3.1.1. CuO-MoO_3 System

The interaction of copper(II) and molybdenum(VI) oxides is known to be accompanied by the formation of molybdates of different composition, depending on the processing/synthesis conditions [22,24,25]. In particular, when an equimolar mixture of copper and molybdenum oxides was heated at 20 K min^{-1} heating rate, a weak endothermic reaction resulted in the formation of the $CuMoO_4$ salt in a quite wide temperature range (743–923 K). When the same mixture was heated at 300 K min^{-1} heating rate (Figure 2) a weak endothermic interaction was observed at higher temperature range (823–903 K) which corresponds to the formation of copper molybdates of different composition (α-$CuMoO_4$, $Cu_3Mo_2O_9$) resolved by XRD analysis (Supplementary Figure S2). In the sample quenched at the mentioned temperature unreacted MoO_3 was observed along with molybdates. Later, at temperatures above 973 K, a wide temperature range of endothermic interactions was observed, which is the sum of several transformations, in particular, corresponding to the continuation of the salt formation process (the amount of molybdenum oxide decreases in the product) and to the modification change of the produced salt (α-$CuMoO_4$ to CuMoO4 III conversion) [26–28]. The complete formation of pure $CuMoO_4$ III was possible to achieve only by non-isothermal heat treatment at high temperature of 1073 K followed by isothermal heat treatment reactive by 10 min (Figure S2E). Meanwhile, under slow heating rate by DTA/TG method (5–20 K min^{-1}) the salt formation ends relatively earlier, at 923 K.

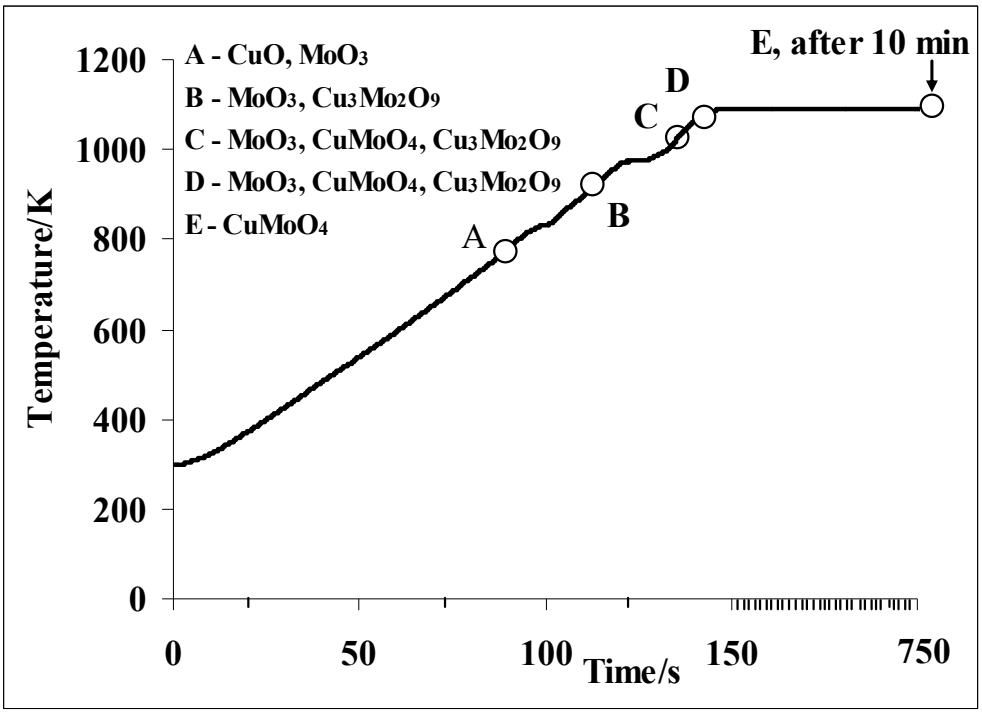

Figure 2. The heating thermogram of the CuO + MoO_3 mixture with the XRD analysis results of the quenched samples at different characteristic temperatures, A—T = 773, B—923, C—1023, D—1073, E—1073 (t_h = 10 min) K, V_h = 300 K min^{-1}.

To complement the aforementioned observations, the IR spectrum was recorded. FTIR (Figure 3) bands of the $CuMoO_4$ were detected at 460, 865 and 965 cm^{-1}. The peak at

865 cm^{-1} is assigned to vibrations of the Mo–O–Mo. The featured peak at 965 cm^{-1} is attributed to Mo = O bond frequency. Furthermore, the absorption peak at 460 cm^{-1} is assigned to superposition of bending mode of MoO_3 lattice and stretching vibration of square planar CuO_4. IR peaks of $Cu_3Mo_2O_9$ and MoO_3 appeared in their fingerprint region at 717 cm^{-1} and 560 cm^{-1}, respectively, match well with the literature data [29,30]. IR peaks on the spectrum at 810 cm^{-1} and 1380 cm^{-1} correspond to in-plane B-N stretching and out-plane B-N-B bending vibrations, respectively, of boron nitride. BN suspension was used to cover the thermocouple wire during HSTS experiments. Some of the bands of $Cu_3Mo_2O_9$ were overlapped (818 cm^{-1}, 902 cm^{-1}, 942 cm^{-1} and 969 cm^{-1}) with the $CuMoO_4$ bands in the 800–1000 cm^{-1} region and were not observed due to their lower intensity compared to $CuMoO_4$ peaks.

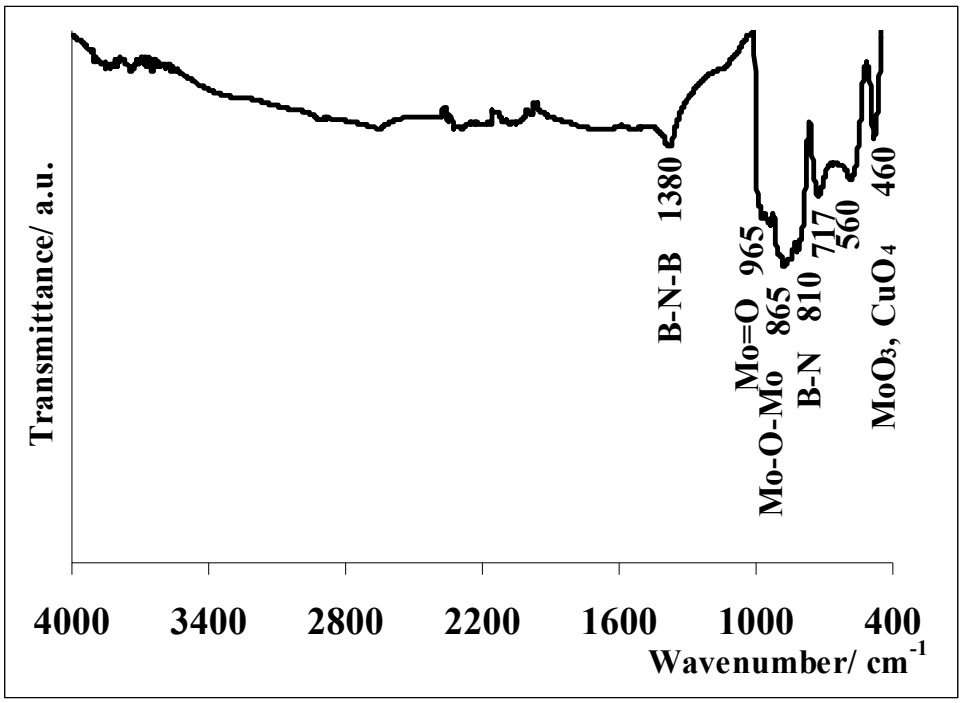

Figure 3. The IR spectrum of the product obtained from CuO + MoO_3 mixture cooled down from 1023 K, V_h = 300 K min^{-1}.

3.1.2. CuO-C System

Carbothermic reduction of copper oxide (CuO + C) is a successive two-stage weak exothermic process (Figure 4). The first stage takes place in the temperature range of 823–973 K and is accompanied by partial reduction of CuO with the formation of Cu_2O (Figure 4B,C and Figure S3B). The second stage begins at temperatures above 973 K and corresponds to the formation of copper from copper suboxide (Figure 4C,D and Figure S3C). The further increase in temperature leads to an increase in the conversion degree and pure copper formation (Figure 4D and Figure S3D).

It is worthy of remark that in the range of low heating rates (5–20 K min^{-1}) a stepwise reduction was also observed, but the interaction was started at a temperature lower by about 100 K [22].

3.1.3. MoO_3-C System

Two weak exothermic and one endothermic peaks arise during the carbothermic reduction of molybdenum (VI) oxide (MoO_3 + 2C) (Figure 5). The process begins with a

weak exothermic interaction (933–1063 K) corresponding to the formation of molybdenum dioxide (Figure S4B) according to the following reaction scheme:

$$MoO_3 + C \rightarrow MoO_2 + CO_2 \text{ (+trace amount of CO) (933–1063 K).}$$

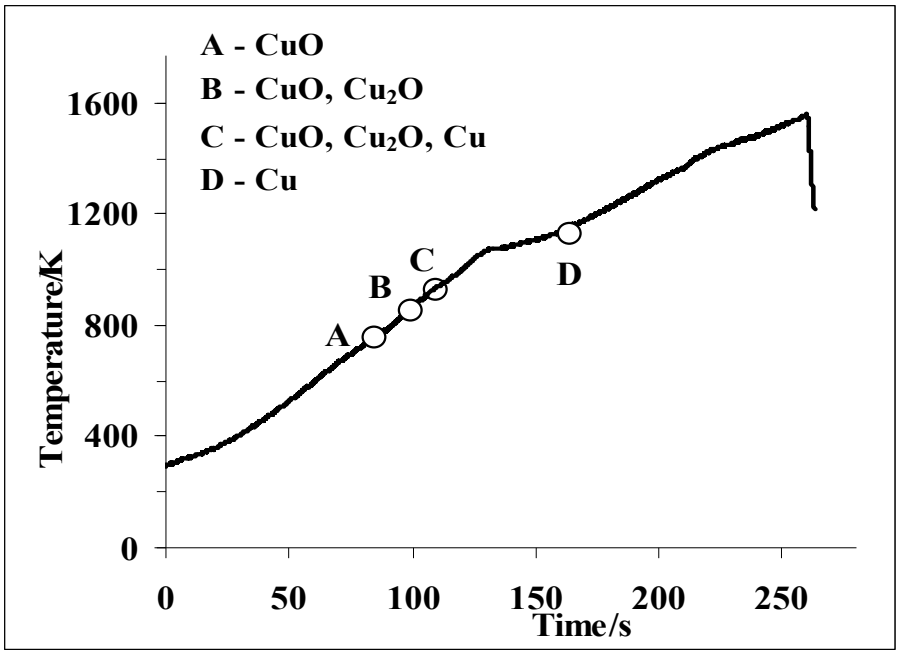

Figure 4. The heating thermogram of the CuO + C mixture with the XRD analysis results of the quenched samples at different characteristic temperatures, A—T = 773, B—873, C—973, D—1153 K, V_h = 300 K min^{-1}.

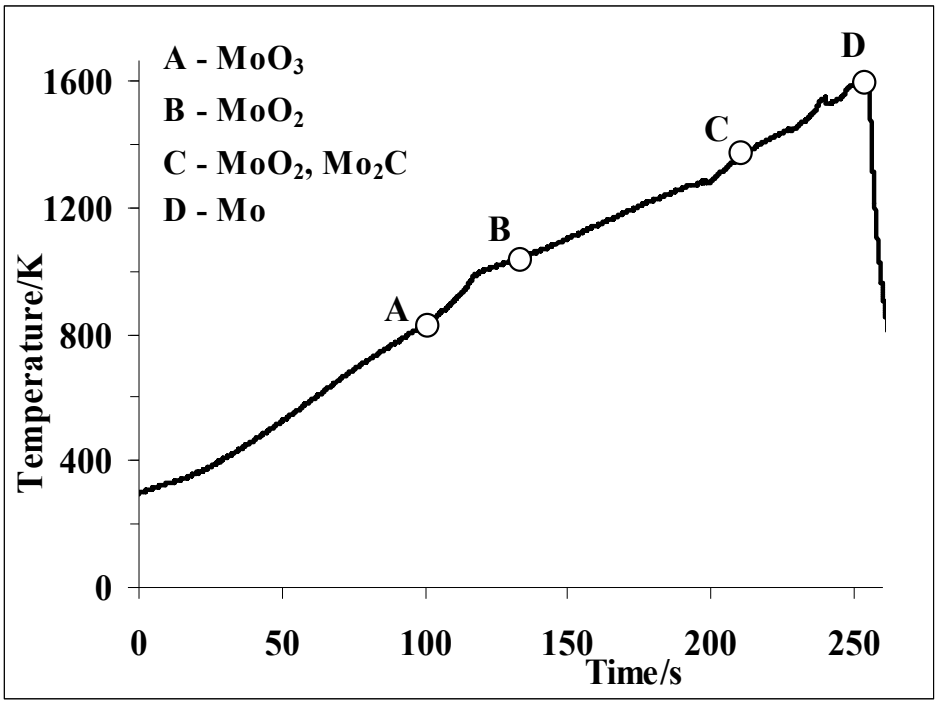

Figure 5. The heating thermogram of the MoO_3 + 2C mixture with the XRD analysis results of the quenched samples at different characteristic temperatures, A—T = 893, B—1063, C—1373, D—1573 K, V_h = 300 K min^{-1}.

Under further heating, the reduction process continues with the residual carbon. In particular, a weak endothermic interaction takes place in the temperature range 1273–1373 K, and in the XRD pattern of the quenched sample MoO_2 and Mo_2C (Figure S4C) are identified as a result of the following interaction:

$$MoO_2 + C \rightarrow Mo_2C + CO/CO_2 \qquad (1273–1373\ K).$$

Further increase in temperature leads to the formation of metallic molybdenum (Figure S4D) according to the following scheme:

$$MoO_2 + Mo_2C \rightarrow Mo + CO/CO_2 \qquad (1483–1573\ K).$$

The carbothermic reduction of molybdenum trioxide at low heating rates (V_h = 20 K min^{-1}) is also a two-step process [31]. Again, the first stage ($MoO_3 \rightarrow MoO_2$) is a weak exothermic reaction (but at lower temperature of 833–953 K), and the second is an endothermic one (>1123 K) accompanied by the formation of metallic molybdenum and/or molybdenum carbide. In contrast to the low heating rates region (5–20 K min^{-1}), at high heating rates (>100 K min^{-1}) these stages are shifted to a higher temperature range, which allows the reduction of metallic molybdenum at high temperature.

3.1.4. MoO_3-Mg System

The magnesiothermic reduction mechanism of MoO_3 + 3Mg mixture was examined in the same range of high heating rates, 100–1200 K min^{-1}. Magnesiothermic reduction of molybdenum oxide over the entire heating rate region occurs with molten magnesium. The increase in the heating rate from 100 up to 1200 K min^{-1} increases characteristic temperatures (T_o, T*, T_{max}). At heating rate of 100–300 K min^{-1} (Figure 6) the interaction initiates just after the melting process of magnesium. In particular, at a heating rate of 300 K min^{-1}, the reduction begins at 943 K along with a severe exothermic peak (943–1058 K) on the heating thermogram with a maximum temperature of 1423 K (T* = 1013 K). Note that the reduction of copper oxide with magnesium began approximately at the same temperature range at 300 K min^{-1} heating rate (953–1073 K, T* = 993 K, T_{max} = 1558 K) [21]. At higher heating rates (600 and 1200 K min^{-1}) the reduction process of MoO_3 begins quite late after the melting of magnesium at temperatures of 1063 and 1083 K, respectively.

The XRD pattern of the sample quenched at a temperature of 923 K (A) contains only characteristic diffraction lines of MoO_3 and Mg (V_h = 300 K min^{-1}) (Figure S5A). Immediately after the exothermic interaction, a partial reduction of molybdenum oxide with the formation of MoO_2 (Figure S5B) is observed. Further increase in temperature leads to molybdenum formation, but, in parallel to the reduction process, the formation of $MgMoO_4$ salt also occurs (Figure S5C,D). However, $MgMoO_4$ is absent at the end of the process, but some unreduced molybdenum dioxide is registered (Figure S5E). Incomplete reduction of molybdenum oxide can be explained by the vigorous interaction and evaporation of magnesium.

3.2. MoO_3-Mg-C, MoO_3-CuO-Mg and MoO_3-CuO-C Ternary Systems

3.2.1. MoO_3-Mg-C System

In the ternary MoO_3-Mg-C system, at low heating rate of 20 K min^{-1}, the interaction began before the melting of magnesium at 833–903 K according to the results reported in [31]. The weak exothermic carbothermic reduction was attributed to the conversion of MoO_3 to MoO_2. The process was further continued with magnesiothermic reduction after the Mg melting up to the formation of metallic molybdenum at 973–1073 K. In contrast to low heating rates, the process begins with the melting of magnesium at 933 K at high heating rates, which is immediately followed by the carbothermic reduction of molybdenum (VI) oxide and lead to the formation of molybdenum dioxide at a temperature of 953–1073 K (Figure 7 and Figure S6).

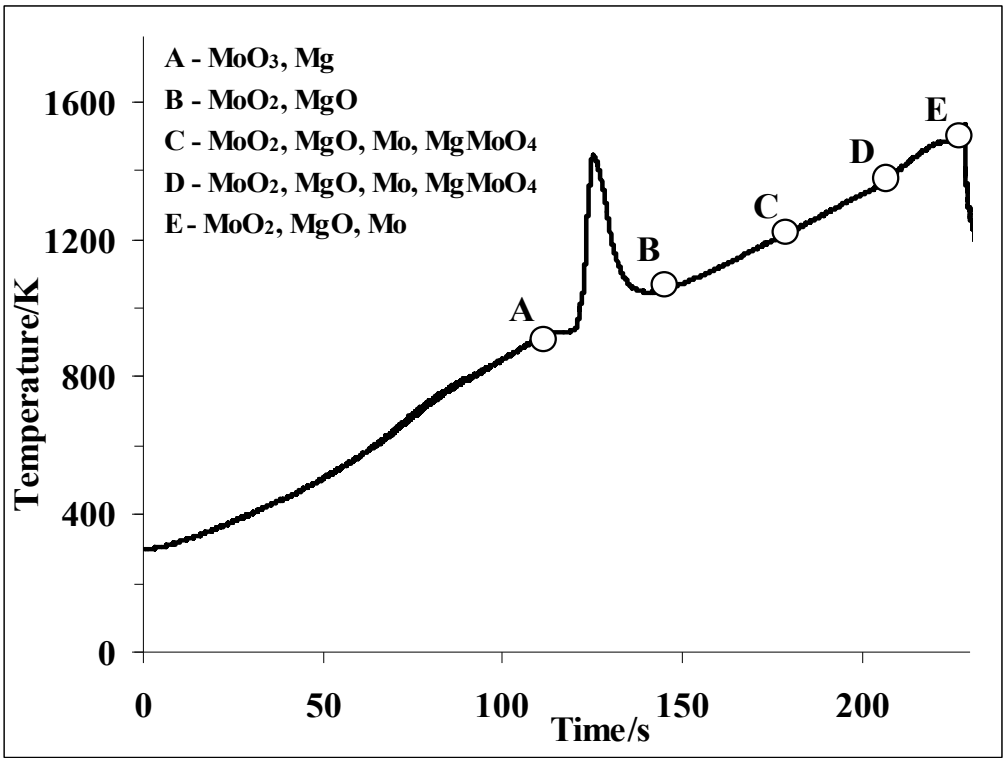

Figure 6. The heating thermogram of the MoO_3 + 3Mg mixture with the XRD analysis results of the quenched samples at different characteristic temperatures, A—T = 923, B—1048, C—1203, D—1323, E—1573 K, V_h = 300 K min^{-1}.

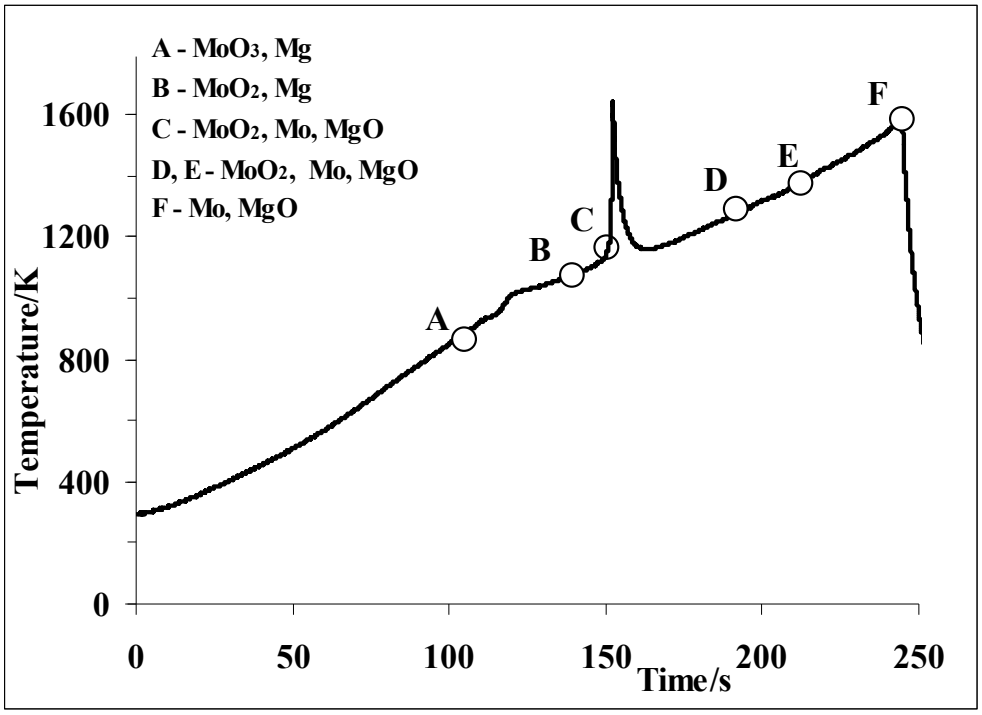

Figure 7. The heating thermogram of the MoO_3 + 1.5Mg + C mixture with the XRD analysis results of the quenched samples at different characteristic temperatures, A—T = 923, B—1073, C—1153, D—1273, E—1423, F—1573 K, V_h = 300 K min^{-1}.

In contrast to the carbothermic reduction of molybdenum (VI) oxide (see Section 3.1.3), utilizing the Mg/C reducing pair, the formation of molybdenum carbide was not observed, and the formation of molybdenum occurs due to a strong exothermic interaction of MoO_2 and magnesium (300 K min^{-1}, 1123–1163 K, T* = 1133 K). The maximum temperature of the magnesio-carbothermic interaction is registered to be 1623 K, which is by ~200 K higher than the temperature recorded during the pure magnesiothermic reduction reaction of molybdenum oxide.

For the comparative overview, one may note, that in the CuO-0.5Mg-0.5C system the interaction began immediately after the melting of magnesium with carbothermic reduction of CuO and accompanied by the formation of copper suboxide. Then magnesium continues the reduction of Cu_2O up to the metallic copper formation [21].

3.2.2. CuO-MoO_3-Mg System

According to the heating thermogram of CuO + MoO_3 + 4Mg mixture, the process of joint magnesiothermic reduction of copper and molybdenum oxides (Figure 8a) is preceded by magnesium melting. The weak endothermic effect observed after magnesium melting is accompanied by the formation of copper molybdate ($Cu_3Mo_2O_9$) at 1073 K, which is immediately followed by the salt reduction process and the formation of metallic copper (1143–1273 K). Metallic molybdenum is formed at a higher temperature range (1273–1373 K). The aforementioned considerations were confirmed by X-ray analysis of the samples quenched at characteristic temperatures, according to which the XRD pattern of the sample interrupted at point C contains $Cu_6Mo_5O_{18}$, $MgMoO_4$, Cu_2O, Cu, Mg (Figure 8b C). At higher temperatures, between 1373 K and 1473 K, there are characteristic peaks of molybdenum and $MgO{\cdot}MoO_2$ mixed oxide as well (Figure 8b D). The latter occurs as a result of the interaction between MgO and MoO_2.

The data derived from the analysis of the heating thermograms revealed that, in contrast to the magnesiothermic reduction of individual oxides, which are highly exothermic interactions (i.e., CuO + Mg with T* = 993 K, T_{max} = 1483 K [21] and MoO_3 + 3Mg with T* = 1013 K; T_{max} = 1428 K), the joint magnesiothermic reduction of oxides (CuO + MoO_3 + Mg) proceeds with weak exothermic stages. As a matter of fact, when two highly exothermic reactions, MoO_3 + 3Mg and CuO + Mg, are carried out together, a slow interaction takes place. This is a typical dysynergistic phenomenon, which comprises a combination of actions, where the effect of the simultaneous action is less than the summation of effects of the individual actions. Dysynergy in the CuO-MoO_3-Mg system may be explained by a dramatic change in the interaction pathway. In particular, as follows from the XRD analysis results of the samples quenched at different stages of the interaction, the reduction process of metal oxides by magnesium is preceded by the formation of $Cu_3Mo_2O_9$ salt (Figure 8b). In addition, the magnesiothermic reduction of $Cu_3Mo_2O_9$ is significantly slower as compared to the reduction of individual oxides. Indeed, according to the XRD data obtained, after the melting of magnesium before the initiation of the reduction process of oxides, a copper molybdate $Cu_3Mo_2O_9$ (at 1073 K) is identified (Figure 8b B) along with copper oxide. This is further followed by the gradual/stepwise reduction of the salt and is accompanied firstly by the formation of Cu, Cu_2O, $MgMoO_4$, $Cu_6Mo_5O_{18}$.

To explain the difference between the combined and separate reduction processes of molybdenum and copper oxides, the magnesiothermic reduction of $CuMoO_4$ salt was studied at similar conditions (300 K min^{-1}) (Figure 9). From the heating curve of the reduction of $CuMoO_4$ by magnesium, two successive and weak exothermic stages were revealed. Similar to the combined magnesiothermic reduction of oxides (after the salt formation process), the melting of magnesium at 923 K is immediately followed by the weak exothermic reduction of copper (943–1153 K), and later the weak exothermic reduction of molybdenum in the temperature range of 1333–1343 K occurs (Figure 9 and Figure S7).

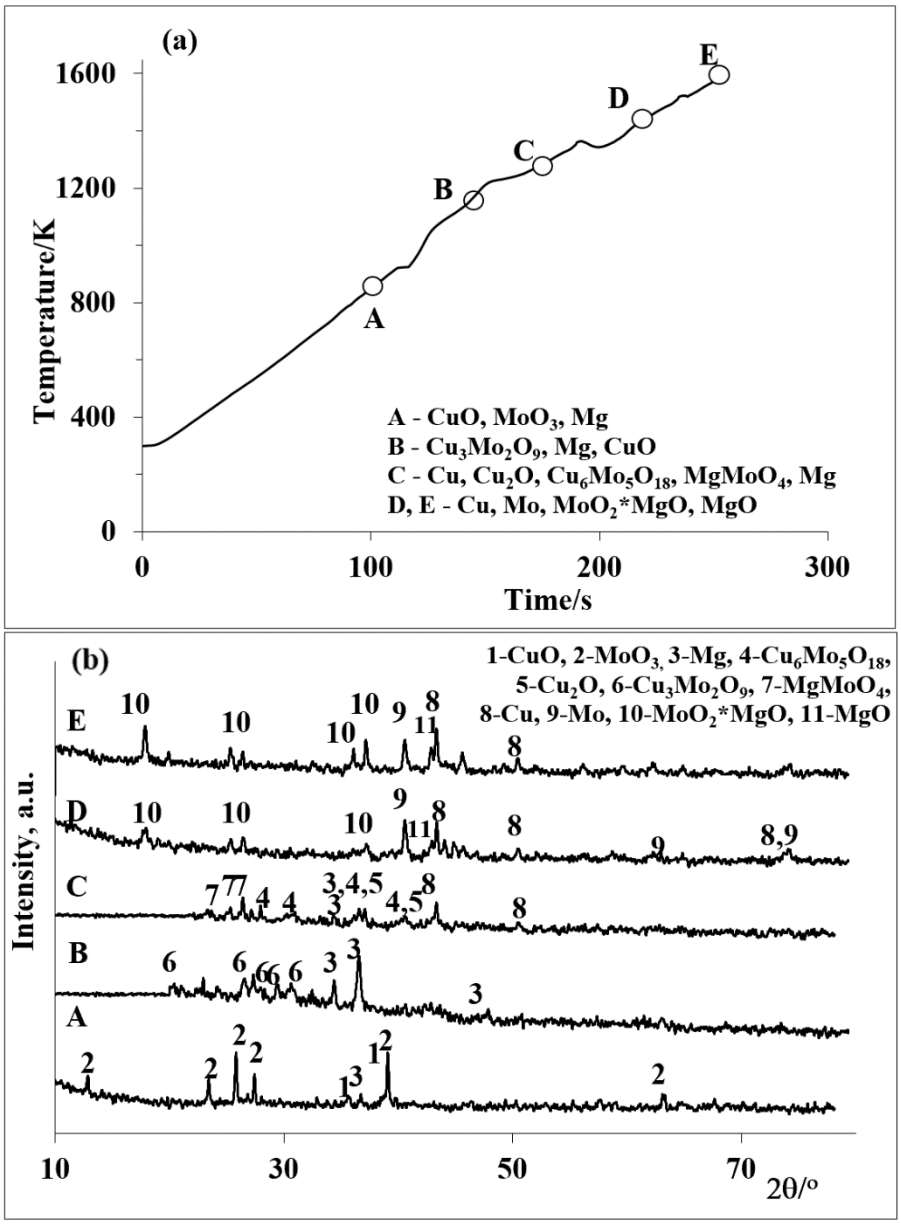

Figure 8. Heating thermogram of the CuO + MoO_3 + 4Mg mixture (**a**) and XRD analysis results (**b**) of the quenched samples at different characteristic temperatures, A—T = 923, B—1143, C—1273, D—1373, E—1473 K, V_h = 300 K min^{-1}.

3.2.3. CuO-MoO_3-C System

In the ternary CuO + MoO_3 + 3C system (Figure 10) the reduction process begins with the weak endothermic reaction of copper molybdate formation (Figure S8B), followed by a weak exothermic interaction. According to XRD analysis results, the complete reduction of copper and partial reduction of molybdenum (Figure S8C) occur during the weak exothermic reaction. Further increase in temperature leads to the formation of molybdenum carbide (Figure S8D, 1273 K). At higher temperatures (T $\geq$ 1423 K), metallic molybdenum is formed due to the interaction of molybdenum carbide and molybdenum dioxide. The sequence of processes in CuO + MoO_3 + 3C system can be represented by the following scheme:

$$MoO_3 + CuO \rightarrow Cu_6Mo_5O_{18} + Cu + MoO_2 \qquad T = 823–913\ K$$

$$Cu_6Mo_5O_{18} + C \rightarrow Cu + MoO_2 + CO/CO_2 \qquad T = 923–1023\ K$$

$$MoO_2 + C \rightarrow Mo_2C + CO/CO_2 \qquad T = 1023–1393\ K$$

$$MoO_2 + Mo_2C \rightarrow Mo + CO/CO_2 \qquad T = 1393–1573\ K$$

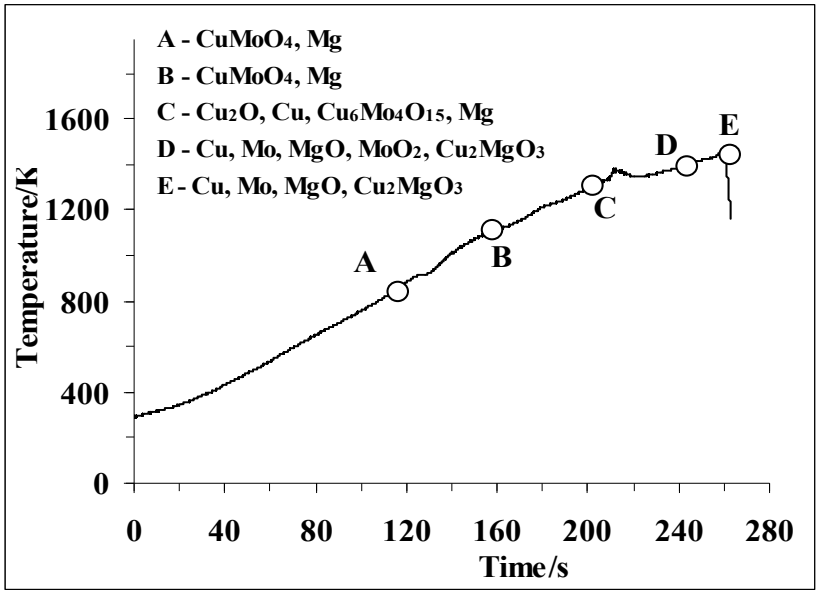

Figure 9. The heating thermogram of the $CuMoO_4$ + 4Mg mixture with the XRD analysis results of the quenched samples at different characteristic temperatures, A—T = 923, B—1123, C—1323, D—1413, E—1573 K, V_h = 300 K min^{-1}.

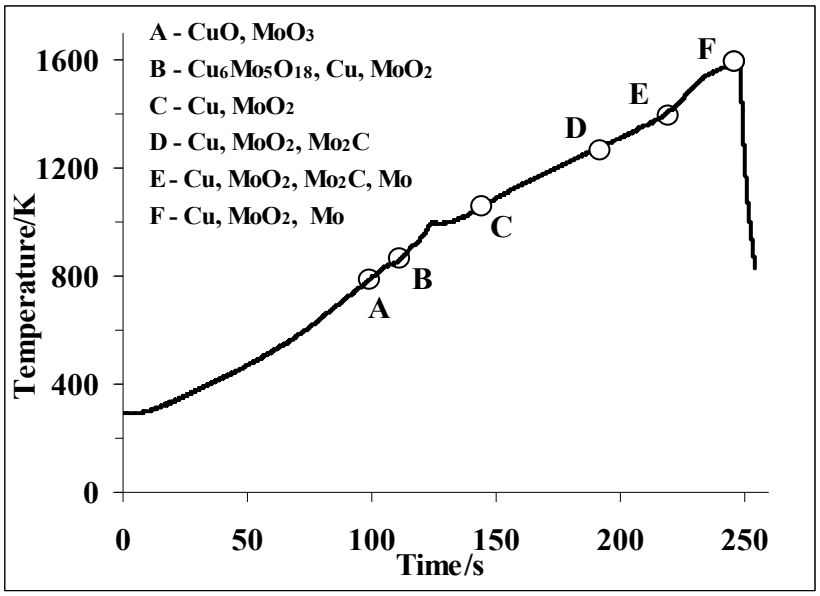

Figure 10. The heating thermogram of the CuO + MoO_3 + 3C mixture with the XRD analysis results of the quenched samples at different characteristic temperatures, A—T = 803, B—913, C—1023, D—1273 E—1393, F—1573 K. V_h = 300 K min^{-1}.

The experimental observations interpreted above imply that the joint reduction of CuO and MoO_3 oxides with separate reducers, such as magnesium or carbon, does not lead to the complete reduction of metals (Mo and Cu).

3.3. CuO-MoO_3-Mg-C Quaternary System

After the detailed consideration of the behavior of the binary and ternary systems, a quaternary system with a composition of CuO + MoO_3 + 1.2Mg + 2.15C was selected.

The ratio of reducers was received from the optimum area of thermodynamic calculations for the joint and complete reduction of Mo and Cu metals [13]. In the selection of the mentioned composition, the combustion synthesis behavior of individual oxides with Mg/C combined reducer was also considered.

In the CuO + MoO_3 + 1.2Mg + 2.15C mixture, the process begins before the magnesium melting, with the carbothermic reduction of copper oxide at temperature up to 873 K (Figure 11a). This is evidenced by the presence of Cu_2O and the absence of MgO in the sample quenched at 873 K (Figure 11b B). During further heating, magnesium melts, and molybdenum oxide is reduced by carbon (MgO is still absent in the product) up to molybdenum dioxide. At a temperature range of 1213–1263 K, the magnesiothermic reduction of MoO_2 occurs with the formation of metallic molybdenum with maximum temperature of 1523 K. The further increase in temperature contributes to the increase in conversion degree (Figure 11b F). The formation of molybdenum carbide by an interaction of the obtained molybdenum and/or molybdenum dioxide with carbon is not excluded.

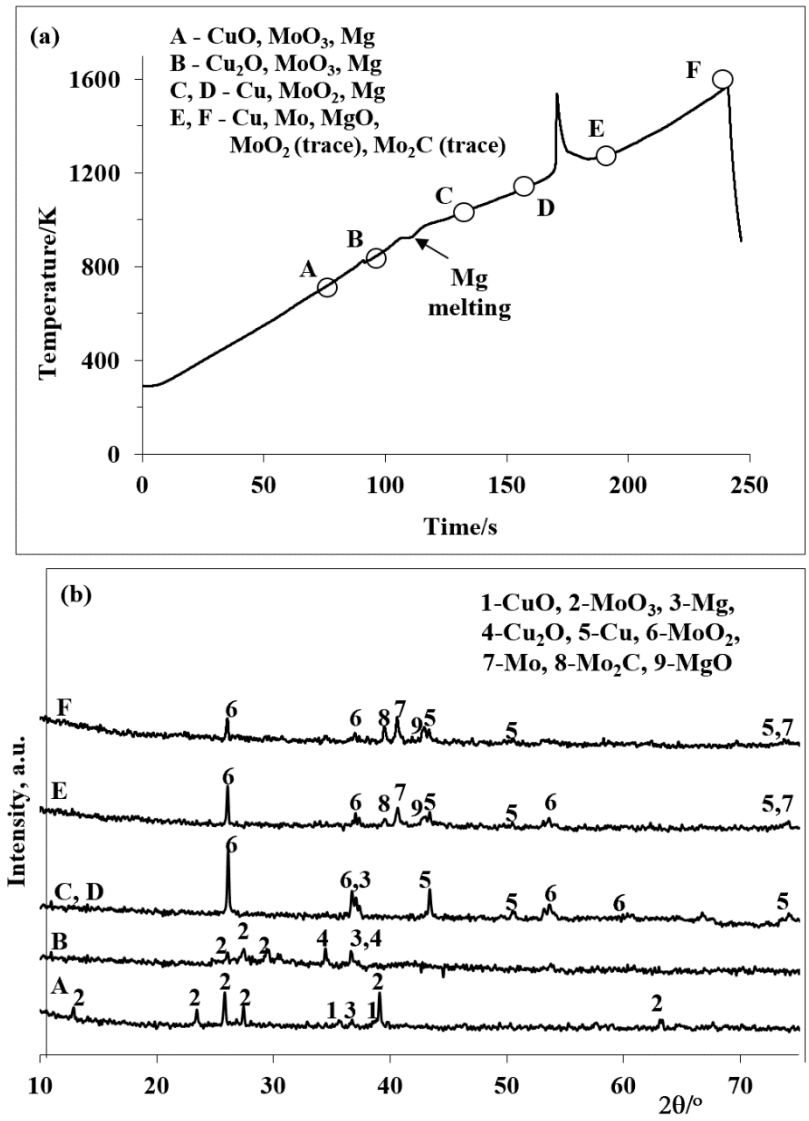

Figure 11. Heating thermogram of the CuO + MoO_3 + 1.2Mg + 2.15C mixture (**a**) and XRD analysis results (**b**) of the quenched samples at different characteristic temperatures, A—T = 773, B—873, C—1023, D—1163, E—1263, F—1573 K, V_h = 300 K min^{-1}.

According to DTA/TG studies conducted at [22] at a heating rate of 20 K min^{-1} in the CuO-MoO_3-Mg-C system, the interaction also begins before the magnesium melting. At 873 K, a parallel reduction of the oxides takes place: copper oxide is reduced to copper via two-step mechanism, and molybdenum oxide to MoO_2. In addition, at low heating rates, the magnesiothermic reduction process of molybdenum dioxide occurs at a lower temperature range: it begins immediately after the melting of magnesium (923 K) and molybdenum formation is observed at 993 K. At the end of the process, the product also contains a complex oxide of MoO_2 and magnesia.

The microstructural analysis of the quaternary CuO + MoO_3 + 1.2Mg + 2.15C mixture (Figure S1), and of the quenched samples at different characteristic temperatures, T = 873 K (Figure 12), T = 1023 K, 1163 K (Figure S9), T = 1263 K, T = 1573 K (Figure 13, Figure 14 and Figure S10) are presented below to demonstrate the microstructure evolution during the high heating conditions. Initial CuO + MoO_3 + 1.2Mg + 2.15C mixture contains monoclinic CuO (outlined orange), orthorhombic MoO_3 (outlined blue), carbon (outlined yellow), magnesium (outlined green).

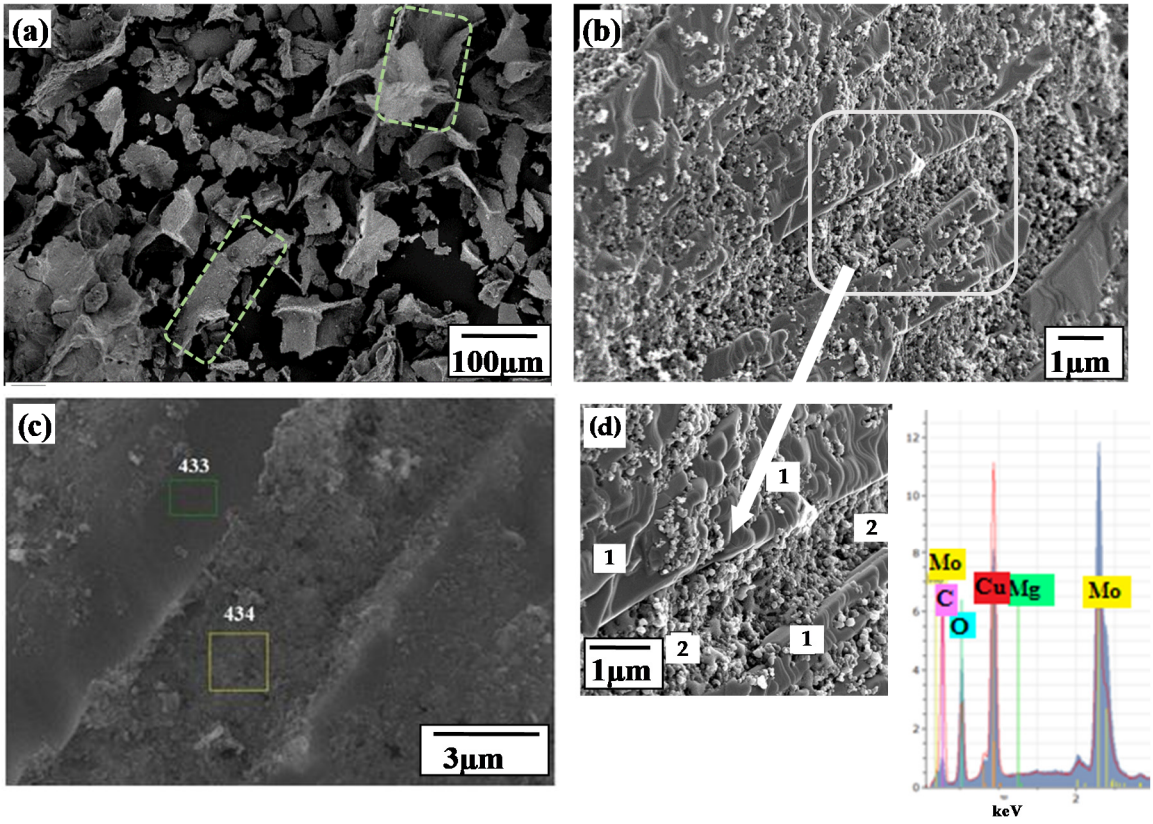

Figure 12. SEMmicrographs of the quenched sample at 873 K at different magnifications (**a**–**c**) and EDS spectra derived from area 1 (or 433—blue) and area 2 (or 434—red) (**d**).

During the heating up to 873 K (before Mg melting) coarse Mg particles are still separately present (Figure 12a, green outlined platelets) and didn't participate in the interaction yet (Figure 12b,c). Another three components appear together in prealloyed state in the form of two different microstructural entities—ribbed laminates (spectrum 433 and points marked 1) and nanospherical agglomerates (spectrum 434 and points marked 2) (Figure 12d). More specifically, according to EDS spectrum (Figure 12e), the alloyed regions (Figure 12c,d spectrum 433) comprise more Mo and O (according to XRD analysis results it should correspond to MoO_3, according to EDS analysis atomic ratio is Mo:O = 1:3.5), and agglomerated particulates (spectrum 434, Figure 12c,d) have more copper and carbon content, and some oxygen is also present (in all probability there are carbon and Cu_2O, which was established also from the XRD patterns). The close contact of copper to carbon

is also complementing to XRD analysis and postulating that CuO reduction up to Cu_2O occurred by carbon.

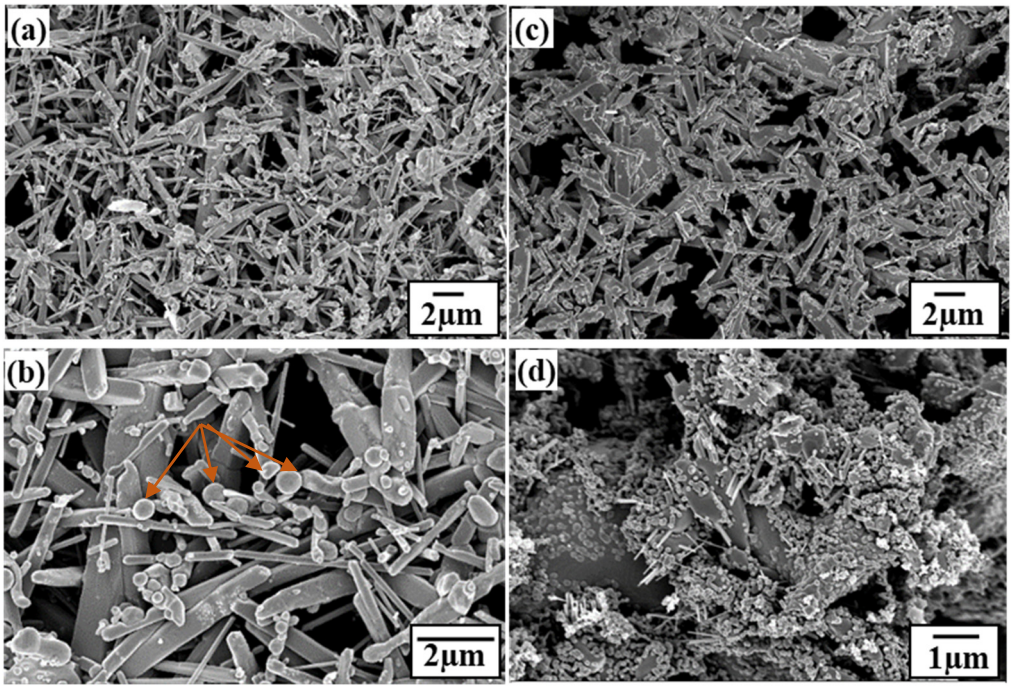

Figure 13. SEM analyses of the quenched sample at 1263 K (**a**,**c**) and 1573 K (**b**,**d**).

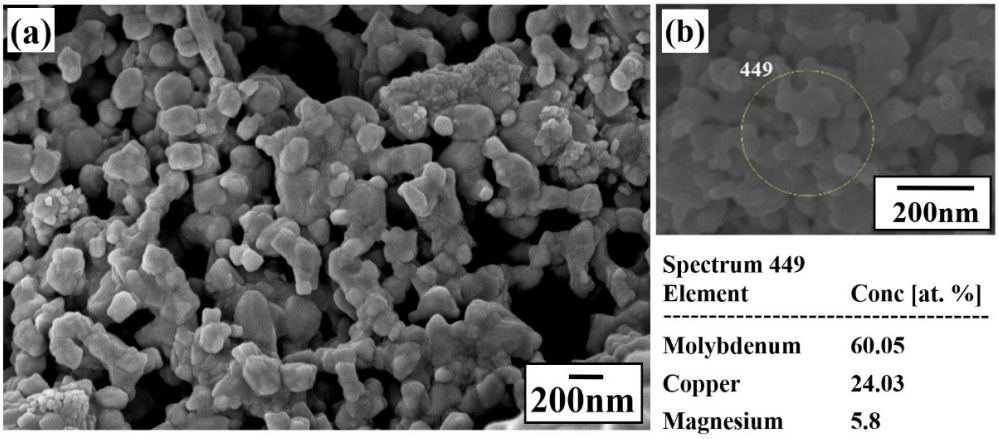

Figure 14. SEM/EDS analyses of the Mo-Cu quenched sample at 1573 K, (**a**,**b**).

After magnesium melting, at 750 °C, microstructural entities were in the form of more homogeneous mixture of molten magnesium and nanoparticles of copper and MoO_2 (Figure S9a,c). At higher temperature (890 °C), two types of MoO_2 are observed (well defined grains and nanospheres), thus mixture undergoes microstructural change without changing phase composition (Figure S9b,d,e). Well-defined grains and nanospheres of MoO_2 are present along with metallic copper and molten magnesium platelets.

The SEM images of samples quenched at 1263 K contain spherical droplets of submicron size (Cu, orange arrows), spherical nanoparticles (Mo-Cu composite with higher molybdenum content), thin nanorods (width up to 100 nm) of light color (MoO_2—spectrum 461 (atomic ratio according to EDS 1:1.8), dark rods of different proportions (Mo from submicron to micron size—spectrum 457), and nanoparticles (spectrum 456) that comprise both Cu and Mo but predominantly molybdenum owing to segregation of molten copper droplets (Figure 13 and Figure S10). At higher temperature, 1573K, microstructure refine-

ment takes place due to the continuation of reduction process from MoO_2 nanorods also by carbon, which leads to the formation of not only molybdenum, but also molybdemum carbide nanoparticles according to $MoO_2 + C \rightarrow Mo_2C + CO/CO_2$ reaction (Figure S10).

In some regions of the sample quenched at 1573 K, Mo and Cu nanoparticles were homogeneously distributed in the nanometer range (Figure 14).

The influence of heating rate was further investigated to understand the formation conditions of byproducts. It was established that regardless the heating rate, the complete reduction of copper oxide and the first stage of reduction of molybdenum trioxide proceed with carbon followed by magnesiothermic or Mg + C combined reduction of MoO_2 (Table 1). In the case of slow heating the process was completed at 1153 K and carbidization was not observed [22], but MoO_2 was present in the quenched product along with target compounds. At high heating rates the process was completed at 1574 K and may be accompanied by the formation of molybdenum carbide.

Table 1. The influence of heating rate on the characteristic temperatures and phase composition of the products of the quaternary CuO-MoO_3-Mg-C system.

V_h, K min^{-1}	The System under Study	T, K	XRD	T, K	XRD	T, K	XRD
20	$CuO + MoO_3$ + + 1.1Mg + 2C	753–793	Cu_2O, MoO_3, Mg	793–873	MoO_2, Cu, Mg	1013–1043 T_{max} = 760	Mo, Cu, MgO, $MgO{\cdot}MoO_2$
100	$CuO + MoO_3$ + + 1.2Mg + 2.15C	773–823	Cu_2O, MoO_3, Mg	923–1003	MoO_2, Cu, Mg	1143–1163 T_{max} = 940	Mo, Cu, MoO_2 (main product), Mo_2C, MgO
300	$CuO + MoO_3$ + + 1.2Mg + 2.15C	833–873	Cu_2O, MoO_3, Mg	933–1013	MoO_2, Cu, Mg	1213–1263 T_{max} = 1523	Mo, Cu, MgO, MoO_2(trace), Mo_2C
2600	$CuO + MoO_3$ + + 1.2Mg + 2.15C	843–883	Cu_2O, MoO_3, Mg	1033–1233	MoO_2, Cu, Mg	1393–1583 T_{max} = 1563	Mo, Cu, MgO, Mo_2C
5200	$CuO + MoO_3$ + + 1.2Mg + 2.15C	853–893	Cu_2O, MoO_3, Mg	1053–1263	MoO_2, Cu, Mg	1403–1633 T_{max} = 1583	Mo, Cu, MgO, Mo_2C(trace)

This difference in the phase composition of the products is conditioned by the difference in heating rates (Table 1), as well as by the difference in maximum temperatures (1153 K vs. 1573 K). In particular, at low heating rates (V_h = 20 K min^{-1}), the product contains molybdenum dioxide together with the main product. At relatively high heating rates (100–1200 K min^{-1}) molybdenum dioxide and molybdenum carbide were observed, and in the heating rate region from 2600–5200 K min^{-1} molybdenum carbide is present in addition to the target materials. In the combustion synthesis, where the heating rate reaches up to 60,000 K min^{-1} [13], the reduction was accomplished with the formation of target substances Mo, Cu, MgO due to utilization of combined reducers in the mixture $CuO + MoO_3$ + 1.2Mg + 2.15C. Considering that combustion synthesis of molybdenum carbide in the solid phase proceeds by the reaction diffusion mechanism, diffusion of carbon through the Mo carbide phase was believed to be the limiting stage of the carbidization process. Thus, it was possible to avoid carbidization reaction during extremely high heating conditions of the combustion wave.

In the $CuO + MoO_3$ + 1.2Mg + 2.15C mixture at the heating rate of 300 K min^{-1} the following sequential processes take place:

$$CuO + C \rightarrow Cu_2O + CO/CO_2, T = 833–943 K$$

$$Cu_2O + C \rightarrow Cu + CO/CO_2, T = 943–1023 K$$

$$MoO_3 + C \rightarrow MoO_2 + CO/CO_2,\ T = 923–1023\ K$$

$$MoO_2 + Mg \rightarrow Mo + MgO,\ T = 1213–1263\ K$$

$$MoO_2 + C \rightarrow Mo_2C + CO/CO_2,\ T > 1173\ K$$

$$Mo + C \rightarrow Mo_2C,\ T > 1173\ K$$

The experimental studies demonstrated that using a combined Mg/C reducer under fast heating conditions confer the possibility to carbon to interact at a lower temperature than magnesium, prevent the salt formation process, which outstrips the reduction process when only the magnesium is used as a reducer. The temperature shift of the reduction process facilitates the joint and complete reduction of the both metals without the noticeable presence of secondary products.

3.4. The Effective Activation Energy of Magnesiothermic Reactions

Based on the results of experiments performed in a wide range of high heating rates (100–1200 K min^{-1}), the effective values of the activation energy for the magnesiothermic reduction stages were calculated by the isoconversional method of Kissinger [32].

The derived expression for determination of activation energy by Kissinger has the following form:

$$\ln\left(\frac{V_h}{\left(T_{max}^{DTA}\right)^2}\right) = \ln A - \frac{E}{R}\left(\frac{1}{T_{max}^{DTA}}\right) \quad (1)$$

where, V_h is the heating rate (K min^{-1}), $T_{max}^{DTA} \equiv T^*$ is the temperature corresponding to the maximum advance in the DTA curve (K), A is the pre-exponential factor, E is the effective activation energy of the process, (kJ mol^{-1}), R is universal gas constant (8.31 J K^{-1} mol^{-1}).

In particular, the activation energy of the magnesiothermic reduction reaction of MoO_3 (Figure 15 (1)) was calculated to be 110 ± 6.9 kJ mol^{-1}, which is about three times less than the E_a value of magnesiothermic reduction of copper oxide ($E_{a(CuO + Mg)}$ = 324 kJ mol^{-1}) [21]. Both values of the activation energy for the MoO_3 + 3Mg and CuO + Mg reactions refer to the reduction process with molten Mg, where $T^* > T_{Mgmelt}$ in the whole range of surveyed heating rates.

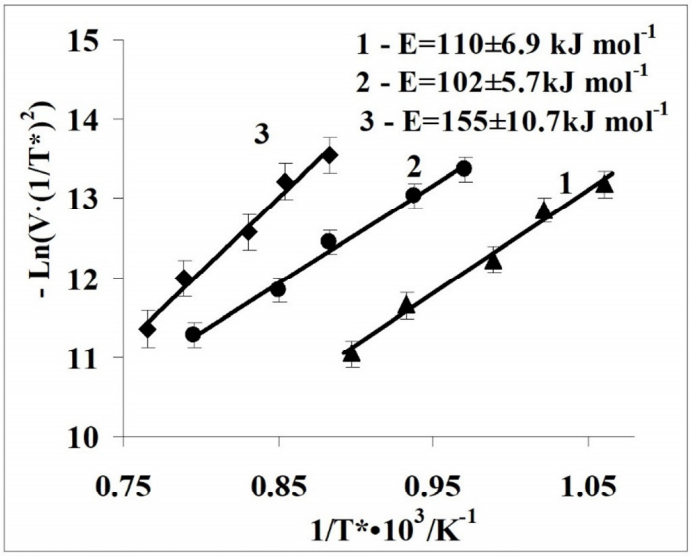

V_h, K min^{-1}	T*, K (1)	(2)	(3)
100	943	1031	1133
150	979	1067	1171
300	1012	1132	1203
600	1073	1175	1267
1200	1115	1257	1307

Figure 15. Linear fitting of the $-\ln(V_h(1/T^*)^2)$ vs. $1/T^* \cdot 10^3$ plot to extract effective activation energy of the magnesiothermic reactions in the MoO_3 + 3Mg (1), MoO_3 + 1.5Mg + C (2), CuO + MoO_3 + 1.2Mg + 2.15C (3) mixtures. V_h = 100–1200 K min^{-1}.

The effective activation energy value of the magnesiothermic reduction stage in the MoO_3 + 1.5Mg + C mixture is 102 ± 5.7 kJ mol^{-1} (Figure 15 (2)), which is commensurate with the activation energy value of magnesiothermic reaction in the MoO_3 + 3Mg mixture stated above (110 ± 6.9 kJ mol^{-1}).

As it was previously delivered in [21], in the CuO + 0.5Mg + 0.5C mixture, the interaction began with carbothermic reduction immediately after melting of magnesium and led to the formation of copper suboxide (Table 2). The reduction of Cu_2O is then continued with magnesium. The activation energy value of Cu_2O + Mg reaction is 320 kJ mol^{-1}, which is approximately three times higher than the activation energy value of the magnesiothermic reduction reaction in the MoO_3 + 1.5Mg + C mixture (Table 2).

Table 2. Comparative overview of the CuO-C, MoO_3-C, CuO-Mg, MoO_3-Mg, CuO-MoO-C, CuO-MoO_3-Mg, CuO-Mg-C, MoO_3-Mg-C, CuO-MoO_3-Mg-C systems at low (20 K min^{-1}) and high (300 K min^{-1}) heating rates.

System [Ref]	V_h/K min^{-1}	Reaction, T/K			E_a/kJ mol^{-1}	Composition		
CuO-Mg [22]	20	843–953			-	Cu, MgO		
CuO-Mg [21]	300	953–1073			424	Cu, MgO		
CuO-C [22]	20	CuO + C 713–803	Cu_2O + C 803–923		-	Cu_2O	Cu	
CuO-C [this work]	300	CuO + C 823–973	Cu_2O + C 973–1153		-	Cu_2O	Cu	
MoO_3-Mg [33]	20	923–973			123	Mo, MgO		
MoO_3-Mg [this work]	300	943–1058			110	Mo, MoO_2, MgO		
MoO_3-C [22,33]	20	MoO_3 + C 773–873	MoO_2 + C 1103–1173		-	MoO_2	Mo	
MoO_3-C [this work]	300	MoO_3 + C 833–953	MoO_2 + C 1123–1373		-	MoO_2	Mo and/or Mo_2C	
CuO-Mg-C [22]	20	CuO + C 703–813	Cu_2O + Mg 923–1063		-	Cu_2O, Mg	Cu, MgO	
CuO-Mg-C [21]	300	CuO + C 923–1023	Cu_2O + Mg 1023–1053		320	Cu_2O, Mg	Cu, MgO	
MoO_3-Mg-C [33]	20	MoO_3 + C 833–903	MoO_2 + Mg 973–1073		197	MoO_2, Mg	Mo, MgO	
MoO_3-Mg-C [this work]	300	MoO_3 + C 953–1073	MoO_2 + Mg 1123–1163		102	MoO_2, Mg	Mo, MgO	
CuO-MoO_3-Mg [22]	20	CuO + MoO_3 823–903	$CuMoO_4$ + Mg 903–1073		-	$CuMoO_4$, Mg, $MgMoO_4$	$Cu_6Mo_5O_{18}$, Mo, MoO_2·MgO, MgO	
CuO-MoO_3-Mg [this work]	300	CuO + MoO_3 940–1073	$Cu_3Mo_2O_9$ + Mg 1143–1273	$Cu_6Mo_5O_{18}$ + Cu_2O + Mg 1273–1373	-	$Cu_3Mo_2O_9$, Mg	Cu, Cu_2O, $Cu_6Mo_5O_{18}$ $MgMoO_4$, Mg	Cu, Mo, MoO_2·MgO, MgO
CuO-MoO_3-C [22]	20	CuO + C 703–803	Cu_2O + MoO_3 + C 803–923		-	Cu_2O, MoO_3	Cu, MoO_2	
CuO-MoO_3-C [this work]	300	CuO + MoO_3 + C 823–913	$Cu_6Mo_5O_{18}$ + MoO_2 + C 923–1023	MoO_2 + C 1023–1393	MoO_2 + Mo_2C 1393–1573	-	$Cu_6Mo_5O_{18}$ Cu, MoO_2	Cu, MoO_2	Mo_2C, MoO_2, Cu	Mo, Cu
CuO-MoO_3-Mg-C [22]	20	CuO + C 753–793	Cu_2O + MoO_3 + C 793–873	MoO_2 + Mg 993–800		-	Cu_2O, MoO_3, Mg	Cu, MoO_2, Mg	Mo, Cu, MgO, MgO·MoO_2
CuO-MoO_3-Mg-C [this work]	300	CuO + C 833–943	Cu_2O + MoO_3 + C 943–1023	MoO_2 + Mg 1213–1263		155	Cu_2O, MoO_3, Mg	Cu, MoO_2, Mg	Mo, Cu, MgO, Mo_2C, MoO_2 (trace)

In the CuO + MoO_3 + 1.2Mg + 2.15C mixture, the activation energy of the magnesiothermic reduction stage (MoO_2 + Mg) is calculated to be 155 ± 10.7 kJ mol^{-1} (Figure 15 (3)).

It is comparatively higher than the E_a value for the MoO_3 + 1.5Mg + C mixture, but about two times lower than E_a value of the CuO + 0.5Mg + 0.5C mixture (102 ± 5.7 kJ mol^{-1} and 320 kJ mol^{-1}, respectively) [21], indicating the change in mechanism of interaction due to joint action of combined reducers.

The values of the effective activation energies calculated for the investigated reactions at high heating rates are presented in Table 2 and collated with the results obtained by DTA/TG method at low heating rates.

According to the data obtained, the magnesiothermic reduction of copper oxide is characterized by the highest value of the activation energy, which decreases when carbon is introduced into the system, thus demonstrating the expediency of utilization of combined reducers.

In MoO_3 + 3Mg and MoO_3 + 1.5Mg + C mixtures, the magnesiothermic reduction is characterized by a lower activation energy value. The energy of activation of joint reduction of oxides with combined reducers is 155 ± 10.7 kJ mol^{-1}, which can be attributed to the magnesiothermic reduction of molybdenum dioxide in the presence of already reduced copper.

4. Conclusions

The study of a separate and joint reduction mechanism of copper and molybdenum oxides with combined reducers (Mg + C) under the fast-heating conditions revealed that, in all the studied systems (CuO-Mg-C, MoO_3-Mg-C, CuO-MoO_3-Mg-C), the reduction process of copper oxide starts at a lower temperature compared to molybdenum oxide. The reduction of copper oxide and copper suboxide proceed exclusively with carbon, while the reduction of molybdenum oxide occurs with both the carbon and magnesium. Moreover, the carbothermic reduction of molybdenum trioxide is accompanied by the formation of MoO_2, which is then reduced to molybdenum by magnesium at higher temperatures. Solely carbothermic reduction of molybdenum trioxide under fast heating conditions obtained pure molybdenum at temperatures above 1473 K. In addition, it was revealed that when two strongly exothermic and violent reactions MoO_3 + 3Mg and CuO + Mg are carried out together, there is a slow interaction with weak self-heating, defined as the dysynergistic phenomenon, which is caused by a total change in the reaction mechanism: the process of Mg-thermic reduction of metals is preceded by the formation of the comparatively stable copper molybdate salt, $CuMoO_4$, and the reduction of the latter proceeds slowly. In the quaternary system, the activation energy value of the magnesiothermic reduction stage is significantly lower than the activation energy values of the magnesiothermic reduction of copper oxide, but only somewhat higher than the E_a value of the magnesiothermic reduction of molybdenum oxide, indicating the expediency of using Mg/C combined reducers. The synergistic influence and reciprocity of combined reducers allows the joint reduction of both metals (Mo, Cu) with trace amounts of byproduct at higher (>2600 K min^{-1}) heating rates.

Supplementary Materials: The following are available online at https://www.mdpi.com/article/10.3390/jcs5120318/s1, Figure S1: SEM analysis of the initial quaternary CuO + MoO_3 + 1.2Mg + 2.15C mixture, Figure S2: XRD patterns of the CuO + MoO_3 mixture; A—T = 773, B—923, C—1023, D—1073, E—1073 (t_h = 10 min) K, V_h = 300 K min^{-1}, Figure S3: XRD patterns of the CuO + C mixture; A—T = 773, B—873, C—973, D—1153 K, V_h = 300 K min^{-1}, Figure S4: XRD patterns of the MoO_3 + 2C mixture; A—T = 893, B—1063, C—1373, D—1573 K, V_h = 300 K min^{-1}, Figure S5: XRD patterns of the MoO_3+3Mg mixture; A—T = 923, B—1048, C—1203, D—1323, E—1573 K, V_h = 300 K min^{-1}, Figure S6: XRD patterns of the MoO_3 + 1.5Mg + C mixture; A—T = 923, B—1073, C—1153, D—1273, E—1423, F—1573 K, V_h = 300 K min^{-1}, Figure S7: XRD patterns of the $CuMoO_4$+4Mg mixture; A—T = 923, B—1123, C—1323, D—1413, E—1573 K, V_h = 300 K min^{-1}, Figure S8: XRD patterns of the CuO + MoO_3 + 3C mixture; A—T = 803, B—913, C—1023, D—1273 E—1393, F—1573 K,

V_h = 300 K min^{-1}, Figure S9. SEM/EDS analyses of the quenched sample at 1023 K (a,c) and 1163 K (b, d, e), Figure S10. SEM/EDS analyses of the quenched sample at 1573 K (a, b, c).

Author Contributions: Conceptualization, H.K., K.N., S.A. and S.K.; data curation, S.K.; funding acquisition, S.A., S.K.; investigation, H.K. and K.N.; methodology, H.K., K.N., S.A.; resources, S.A., S.K.; supervision, S.A., S.K.; visualization, H.K.; writing—original draft, H.K.; writing—review and editing, H.K., S.A. and S.K. All authors have read and agreed to the published version of the manuscript.

Funding: This research was funded by the Committee of Science Ministry of Education, Science, Culture and Sports of the Republic of Armenia (grant numbers 13–1D192, 20TTWS-2F040, 20RF-154), and the Estonian Research Council (S.A.) (grant number PSG220).

Institutional Review Board Statement: Not applicable.

Informed Consent Statement: Not applicable.

Data Availability Statement: The authors confirm that the data supporting the findings of this study are available within the article.

Acknowledgments: This work was supported by the Committee of Science Ministry of Education, Science, Culture and Sports of the Republic of Armenia (grant numbers 13–1D192, 20TTWS-2F040, 20RF-154), and the Estonian Research Council (S.A.) (grant number PSG220). The authors would like to thank also Olga Volubujeva for her help with SEM/EDS analyses.

Conflicts of Interest: The authors declare no conflict of interest.

References

1. Phasha, M.; Bolokang, A.; Kebede, M. First-principles investigation of W V and W Mo alloys as potential plasma facing materials (PFMs) for nuclear application. *Int. J. Refract. Met. Hard Mater.* **2021**, *95*, 105448. [CrossRef]
2. Yang, X.; Qiu, W.; Chen, L.; Tang, J. Tungsten–potassium: A promising plasma-facing material. *Tungsten* **2019**, *1*, 141–158. [CrossRef]
3. Zhang, J.; Shen, Q.; Luo, G.; Li, M.; Zhang, L. Microstructure and bonding strength of diffusion welding of Mo/Cu joints with Ni interlayer. *Mater. Des.* **2012**, *39*, 81–86. [CrossRef]
4. Shokrvash, H.; Rad, R.Y.; Massoudi, A.; Shokrvash, R. Copper Bimetals and Their Nanocomposites. In *Nanorods and Nanocomposites*; IntechOpen: London, UK, 2020. [CrossRef]
5. Agostinetti, P.; Palma, M.D.; Bello, S.D.; Heinemann, B.; Nocentini, R.; Zauner, C.; Langer, H.; Klammer, J. Investigation of the thermo-mechanical properties of electro-deposited copper for ITER. *J. Nucl. Mater.* **2011**, *417*, 924–927. [CrossRef]
6. Souli, I.; Gruber, G.C.; Terziyska, V.L.; Zechner, J.; Mitterer, C. Thermal stability of immiscible sputter-deposited Cu-Mo thin films. *J. Alloys Compd.* **2019**, *783*, 208–218. [CrossRef]
7. Kumar, A.; Jayasankar, K.; Debata, M.; Mandal, A. Mechanical alloying and properties of immiscible Cu-20 wt.% Mo alloy. *J. Alloys Compd.* **2015**, *647*, 1040–1047. [CrossRef]
8. Souli, I.; Terziyska, V.L.; Zechner, J.; Mitterer, C. Microstructure and physical properties of sputter-deposited Cu-Mo thin films. *Thin Solid Films* **2018**, *653*, 301–308. [CrossRef]
9. Zhang, H.; Cao, W.-C.; Bu, C.-Y.; He, K.; Chou, K.-C.; Zhang, G.-H. Sintering behavior of molybdenum-copper and tungsten-copper alloys by using ultrafine molybdenum and tungsten powders as raw materials. *Int. J. Refract. Met. Hard Mater.* **2020**, *88*, 105194. [CrossRef]
10. Zhu, W.; Wang, X.; Liu, C.; Zhou, Z.; Wu, F. Formation and homogenisation of Sn Cu interconnects by self-propagated exothermic reactive bonding. *Mater. Des.* **2019**, *174*, 107781. [CrossRef]
11. Vogel, K.; Braun, S.; Hofmann, C.; Weiser, M.; Wiemer, M.; Otto, T.; Kuhn, H. Reactive Bonding. In *3D and Circuit Integration of MEMS*; Wiley: Hoboken, NJ, USA, 2021; pp. 309–329. [CrossRef]
12. Pascal, C.; Marin-Ayral, R.; Tédenac, J. Joining of nickel monoaluminide to a superalloy substrate by high pressure self-propagating high-temperature synthesis. *J. Alloys Compd.* **2002**, *337*, 221–225. [CrossRef]
13. Aydinyan, S.; Kirakosyan, H.; Kharatyan, S. Cu–Mo composite powders obtained by combustion–coreduction process. *Int. J. Refract. Met. Hard Mater.* **2016**, *54*, 455–463. [CrossRef]
14. Minasyan, T.; Kirakosyan, H.; Aydinyan, S.; Liu, L.; Kharatyan, S.; Hussainova, I. Mo–Cu pseudoalloys by combustion synthesis and spark plasma sintering. *J. Mater. Sci.* **2018**, *53*, 16598–16608. [CrossRef]
15. Kharatyan, S.L. High speed temperature scanner (HSTS) for nonisothermal kinetic studies. In Proceedings of the III International Conference on Nonisothermal Phenomena and Processes: From Thermal Explosion Theory to Structural Makrokinetics, Chernogolovka, Russia, 28–30 November 2016; pp. 22–23.
16. Zakaryan, M.; Nazaretyan, K.; Aydinyan, S.; Kharatyan, S. Joint Reduction of NiO/WO_3 Pair and $NiWO_4$ by Mg + C Combined Reducer at High Heating Rates. *Metals* **2021**, *11*, 1351. [CrossRef]

17. Zakaryan, M.K.; Nazaretyan, K.T.; Aydinyan, S.V.; Kharatyan, S.L. NiO reduction by Mg + C combined reducer at high heating rates. *J. Therm. Anal. Calorim.* **2021**, *146*, 1811–1817. [CrossRef]
18. Hobosyan, M.A.; Kirakosyan, K.G.; Kharatyan, S.L.; Martirosyan, K.S. PTFE–Al2O3 reactive interaction at high heating rates. *J. Therm. Anal. Calorim.* **2015**, *119*, 245–251. [CrossRef]
19. Porter, D.A.; Easterling, K.E. *Phase Transformations in Metals and Alloys (Revised Reprint)*, 3rd ed.; Taylor & Francis Group: New York, NY, USA, 2009; p. 520.
20. Massih, A.R.; Jernkvist, L.O. Solid state phase transformation kinetics in Zr-base alloys. *Sci. Rep.* **2021**, *11*, 1–16. [CrossRef]
21. Aydinyan, S.V.; Nazaretyan, K.T.; Zargaryan, A.G.; Tumanyan, M.E.; Kharatyan, S.L. Reduction mechanism of WO3 + CuO mixture by combined Mg/C reducer. *J. Therm. Anal. Calorim.* **2018**, *133*, 261–269. [CrossRef]
22. Kirakosyan, H.; Minasyan, T.; Niazyan, O.; Aydinyan, S.; Kharatyan, S. DTA/TG study of CuO and MoO3 co-reduction by combined Mg/C reducers. *J. Therm. Anal. Calorim.* **2016**, *123*, 35–41. [CrossRef]
23. Aydinyan, S.V.; Manukyan, K.V.; Kharatyan, S.L. Combustion synthesis of Mo–Cu nanocomposites by co-reduction of molybdenum and copper oxides. In Proceedings of the XII International Symposium on SHS, South Padre Island, TX, USA, 21–24 October 2013; pp. 100–101.
24. Minasyan, T.T.; Aydinyan, S.V.; Kharatyan, S.L. Combustion synthesis of Mo-Cu composite powders from oxide precursors with various proportions of metals. *Chem. J. Armen.* **2016**, *69*, 47–57.
25. Moffatt, W.G. *The Handbook of Binary Phase Diagrams General Electric Company*; Corporate Research and Development, Technology Marketing Operation, The Materials Informations Society, ASM International: Novelty, OH, USA, 1981; Volume 3, p. 522.
26. Wiesmann, M.; Ehrenberg, H.; Miehe, G.; Peun, T.; Weitzel, H.; Fuess, H. p–TPhase Diagram of $CuMoO_4$. *J. Solid State Chem.* **1997**, *132*, 88–97. [CrossRef]
27. Ehrenberg, H.; Weitzel, H.; Paulus, H.; Wiesmann, M.; Wltschek, G.; Geselle, M.; Fuess, H. Crystal structure and magnetic properties of $CuMoO_4$ at low temperature (γ-phase). *J. Phys. Chem. Solids* **1997**, *58*, 153–160. [CrossRef]
28. Tali, R.; Tabachenko, V.V.; Kovba, L.M.; Dem'yanets, L.N. The crystal strucure of $CuMoO_4$-III. *Russ. J. Inorg. Chem.* **1991**, *36*, 927–928.
29. Saravanakumar, B.; Ravi, G.; Yuvakkumar, R.; Ganesh, V.; Guduru, R.K. Synthesis of polyoxometalates, copper molybdate ($Cu_3Mo_2O_9$) nanopowders, for energy storage applications. *Mater. Sci. Semicond. Process.* **2019**, *93*, 164–172. [CrossRef]
30. Lin, Z.; Zhang, X.; Liu, S.; Zheng, L.; Bu, Y.; Deng, H.-H.; Chen, R.; Peng, H.; Lin, X.; Chen, W. Colorimetric acid phosphatase sensor based on MoO_3 nanozyme. *Anal. Chim. Acta* **2020**, *1105*, 162–168. [CrossRef] [PubMed]
31. Manukyan, K.; Aydinyan, S.; Aghajanyan, A.; Grigoryan, Y.; Niazyan, O.; Kharatyan, S. Reaction pathway in the MoO_3+Mg+C reactive mixtures. *Int. J. Refract. Met. Hard Mater.* **2012**, *31*, 28–32. [CrossRef]
32. Kissinger, H.E. Variation of peak temperature with heating rate in differential thermal analysis. *J. Res. Natl. Bur. Stand.* **1956**, *57*, 217. [CrossRef]
33. Baghdasaryan, A.; Niazyan, O.; Khachatryan, H.; Kharatyan, S. DTA/TGA study of molybdenum oxide reduction by Mg/Zn & Mg/C combined reducers at non-isothermal conditions. *Int. J. Refract. Met. Hard Mater.* **2015**, *51*, 315–323. [CrossRef]